Published in final edited form as:
Nat Photonics. 2018 December ; 12(12): 749–753. doi:10.1038/s41566-018-0281-6.

Microwave plasmonic mixer in a transparent fibre-wireless link

Y. Salamin[1,*], **B. Baeuerle**[1], **W. Heni**[1], **F. C. Abrecht**[1], **A. Josten**[1], **Y. Fedoryshyn**[1], **C. Haffner**[1], **R. Bonjour**[1], **T. Watanabe**[1], **M. Burla**[1], **D. L. Elder**[2], **L. R. Dalton**[2], and **J. Leuthold**[1,*]

[1]ETH Zurich, Institute of Electromagnetic Fields (IEF), 8092 Zurich, Switzerland [2]University of Washington, Department of Chemistry, Seattle, WA 98195-1700, USA

Abstract

To cope with the high bandwidth requirements of wireless applications1, carrier frequencies are shifting towards the millimetre-wave and terahertz bands2–5. Conversely, data is normally transported to remote wireless antennas by optical fibres. Therefore, full transparency and flexibility to switch between optical and wireless domains would be desirable6,7. Here, we demonstrate for the first time a direct wireless-to-optical receiver in a transparent optical link. We successfully transmit 20 and 10 Gbit/s over wireless distances of 1 and 5 m at a carrier frequency of 60 GHz, respectively. Key to the breakthrough was a plasmonic mixer directly mapping the wireless information onto optical signals. The plasmonic scheme with its subwavelength feature and pronounced field confinement provides a built-in field enhancement of up to 90’000 over the incident field in an ultra-compact and CMOS compatible structure. The plasmonic mixer is not limited by electronic speed and thus compatible with future terahertz technologies.

Keywords

Plasmonics; terahertz; microwave photonics; optical communications; modulator; field enhancement; nonlinear optics; field enhancement

High-capacity millimetre-wave (MMW) and terahertz (THz) links require efficient transmitters and receivers. In this context, photonics – or microwave photonics – has emerged as a successful approach to overcome electronic related speed limitations2,3,7. And

[*]**Correspondence and requests for materials** should be addressed to Y.S. or J.L. yannick.salamin@ief.ee.ethz.ch, juerg.leuthold@ief.ee.ethz.ch.

Data availability. The data that support the plots within this paper and other findings of this study are available from the corresponding author upon reasonable request.

Author Contributions

Y.S conceived the concept, designed and fabricated the device, designed and performed the experiments and analysed the data. B.B., F.C.A. and A.J. performed the data experiment and data analysis. W.H. fabricated the device, developed the poling process and contributed to the measurements. Y.F. fabricated the device. C.H. contributed to the design of the device and experiment. R.B. and M.B. contributed to the design of the experiment. T.W contributed to the design of the device. D.L.E. & L.R.D. developed and synthesized the HD-BB-OH/YLD124 nonlinear material. J.L. conceived the concept and supervised the project. All authors have contributed to the writing of the manuscript.

Competing interests

The authors declare no competing interest.

Europe PMC Funders Author Manuscripts

indeed, the community has come up with most efficient optical-to-wireless transmitters that work reliably up to 400 GHz8–10. Furthermore, fully integrated transmitters have been demonstrated11–13. However, the reception of wireless signals and the direct up-conversion to an optical signal has turned out to be a challenge to this very day.

Until now, wireless-to-optical receiver systems mainly rely on high-speed electronics14. Usually, the signal is received by an antenna, pre-amplified, and mixed down to the baseband or to an intermediary frequency with an electronic mixer. After an additional amplification stage, the signal is converted to the optical domain by means of an electro-optic modulator7. Therefore, a simple solution that would allow a direct wireless-to-optical conversion (omitting electronics) is of great interest – particularly if realized on a low-cost platform such as silicon15. A possible application scenario in access networks6 is depicted in Fig. 1.

Recently, a wireless-to-optical conversion without RF down-mixing was demonstrated over a distance of 4 meters16. 10 GBd 16 QAM signals from two external antennas were separately amplified and then converted back to the optical domain by a dual-polarization modulator. This approach is interesting, yet, an electro-optic device capable of directly converting the wireless signal to the optical domain would strongly reduce the complexity, cost, and bulkiness of MMW and THz receivers. Most importantly, an electro-optical approach wouldn't require any high frequency RF front-end electronics which would ultimately limit the RF carrier frequency by the electronic speed. Surely, several direct wireless-to-optical converters with an antenna directly combined with an optical modulator have been demonstrated17–20. For instance, successful photonics based electro-optic conversion of 60 GHz and 14 GHz sinusoidal carriers were demonstrated over distances of 25 cm and 40 cm, respectively. These demonstrations used respectively nonlinear optical materials such as lithium niobate17 or organic polymer20. Recently, a direct RF-photonic receiver at 36 GHz with a 1 MBd 64 QAM signal for a 23 cm link was demonstrated19. While these are most interesting approaches, it is clear that the current approaches either suffer from electro-optical bandwidth limitations that makes a transition to higher carrier frequencies difficult or that they require a way more sensitive reception that would allow a higher modulation. In parallel, plasmonics21 has emerged as a field that offers almost unlimited bandwidth22 and impressive modulation depths at very low electrical fields23 thanks to their subwavelength confinement capabilities24. These unique features make plasmonic electro-optic phase modulators an ideal candidate for the direct wireless-to-optical conversion up to THz frequencies18,25. Recently, it was shown that combining a plasmonic electro-optic phase modulator26 with a dipole antenna, a 60 GHz signal could be mapped to the optical domain with high conversion efficiency27.

Here, we demonstrate a direct wireless-to-optical conversion with a plasmonic phase modulator directly integrated with a resonant four-leaf-clover (4LC) antenna. The performance of the converter is shown in a 20 Gbit/s and 10 Gbit/s line-rate experiment at a 60 GHz carrier over the free-space distances of 1 and 5 m, respectively. No RF front-end electronics was required in the wireless to optical receiver because the scheme offers an inherent built-in plasmonic field enhancement up to 90'000. The complete electro-optic device requires only 0.315 mm^2 of footprint, is scalable from GHz to THz and fabrication is

compatible with standard silicon technologies. Not only can such a device pave the path for new applications, but may give way to new array systems such as needed for high data-rate beam steering7.

The device, shown in Fig. 2a, consists of a millimetre-wave antenna and a plasmonic phase modulator combined in one single metallic structure. Light guided by silicon (Si) waveguides is converted to and from surface plasmon polaritons (SPPs) by photonic-plasmonic converters26. The SPPs propagate along the plasmonic modulator formed by a horizontally aligned metal-insulator-metal (MIM) slot waveguide28 filled with a nonlinear organic material29. When an incident MMW field couples to the resonant antenna, charge carriers oscillate with the incident field producing an electric field across the MIM slot. As the metallic antenna arms are used to form the plasmonic MIM slot, all the voltage drop occurs across the nonlinear material. Due to the Pockels effect, the refractive index of the nonlinear material in the slot changes linearly with the incident MMW field strength (see methods section). This way, a wireless signal can directly modulate the phase of a SPP propagating along the slot.

The proposed structure can efficiently convert wireless signals to the optical domain for mainly three reasons. First, the nano-scale slot provided by plasmonics gives rise to a strong field enhancement due to the inverse dependency of the field with the slot width. Second, the resulting electric field in the slot overlaps almost perfectly with the optical field propagating along the MIM slot waveguide leading to a strong nonlinear interaction (see supplementary information, S1). Third, the resonant nature of the 4LC antenna further enhances the electric field in the slot and is maximized by fulfilling the full-wave resonance condition30 (see supplementary information, S2). In this respect, a trade-off between achievable field enhancement and the available bandwidth limits the design. Even though the wavelength of the 60 GHz carrier is 5 mm in free-space, due to the high-k silicon substrate the dimensions of the antenna can be below mm^2, which is a benefit for integration.

Devices were fabricated on a SOI wafer, see Fig. 2a (see methods section). The electro-optic conversion efficiency of the device has been tested first. From the measured modulation depth (see methods section), one can calculate the field enhancement achieved by the structure27. As expected a slot width dependency is observed, see Fig. 2b (blue marks). Although highest FE is achieved for narrow slots, the insertion losses and poling efficiency play a role in the overall conversion performance and have slot width dependency as well31. The optimal slot width is found to be around 75 nm. A field enhancement of up to 60’000 was found for the device with the 75 nm wide plasmonic slot, see blue squares (tagged by 4LC Antenna). The device with a back reflector (BR) has an increased FE of 90’000, see red square (tagged 4LC Antenna with Back Reflector). Comparing the FE of a simple dipole antenna structure (yellow square) with the 4LC Antenna, a clear increase in the efficiency can be observed for the 4LC structures. The bandwidth around the 60 GHz carrier was measured and found to be 3.1 GHz (see Fig. 2c), close to the expected value of the designed resonant antenna. This corresponds to a relative bandwidth of 5%. The antenna with back-reflector had an increased relative bandwidth of 10%. This is slightly less than the relative bandwidth of 12% e.g. available in Ref 16. However, the relative bandwidth in our approach can be adapted by choosing another resonant structure. So for instance, a dipole antenna can

provide relative bandwidths beyond 25%27,32. Figure 2d shows the modulation depth achievable as a function of the power intensity at the receiver. A linear dependency is observed, and strong modulation can be achieved even with reasonable transmitted power. A modulation index of 0.2 rad is easily achieved for a wireless distance of 5 m. Such a modulation index corresponds to an equivalent applied voltage of 0.8 V, and is sufficient for high-data-rate modulation23.

To test the device in a last meter scenario as depicted in Fig. 1, a transparent fibre-wireless-fibre link has been built, as shown in Fig. 3 (see supplementary information, S3). First the electrical data consisting of a quadrature phase shift keying (QPSK) signal with a random bit sequence of length 40960 is encoded on an optical carrier (f_0) by means of an IQ-modulator (Optical Tx). Ultimately, it is the goal to transmit multiple of 10 Gbit/s – which is a standard in datacom and FTTH. Subsequently, the optical signal is converted to a millimetre-wave wireless signal (RF Tx) by a heterodyne approach (see methods section). The wireless signal is focused on the passive plasmonic mixer by means of a high density polyethylene (HDPE) lens and converted back on an optical carrier (f_0-f_{RF}). Finally, the electrical signal is recovered in a coherent optical receiver (Optical Rx). The wireless link between the transmitter and receiver was tested in a 1 m and 5 m scenario with two different 4LC devices with and without back reflector, respectively.

The results of the fibre-wireless-fibre data experiment are shown in Fig. 4. Line rates of 2 and up to 20 Gbit/s were achieved for the 1 m link with bit-error ratios (BERs) of 1.6×10^{-5} to 3.1×10^{-3}, and line rates of 4 Gbit/s and up to 10 Gbit/s for a 5 m link with BERs of 1.6×10^{-5} to 2.3×10^{-3}. Note that no electronics was used in the passive wireless-to-optical receiver. Errors in signals with a BERs below the hard-decision forward error correction (HD-FEC) limit33 of 4.5×10^{-3} can be corrected with a small overhead of 7%.

To assess the limits and opportunities of the proposed plasmonic mixer technology one can resort to the bandwidth distance product as a figure of merit (FOM). The bandwidth and distance are defined respectively by the 3 dB electro-optic bandwidth times the distance at which the achievable BER stays below the HD-FEC limit. With this FOM we obtain for the first experiment (1 m link) a 6 GHz·m and in the second experiment (5 m link) a 15 GHz·m bandwidth-distance products. These numbers need to be taken with care though as they do not show what is really possible. For instance, the Tx and Rx antenna link gain in our setup account for a 56 dBi gain, whereas in literature schemes with more than 86 dBi are frequently used4,8,34. This would leave a margin of more than 30 dB of link gain if needed. Also, in our first chip generations we report fibre-to-fibre losses of 44 and 34 dB for the two generations of devices. These optical losses are high. Yet, by resorting to fibre-to-chip schemes offered by foundries35 and by exploiting the most recent resonant plasmonic structures36 the overall chip losses can be as low as 8 dB (see methods section). There is thus a 26 dB of optical link gain – corresponding to a 52 dB of electrical gain that one can still take advantage of. Lastly, the scheme is scalable to higher carrier frequencies such as e.g. 300 GHz. This is possible since the frequency response of the plasmonic modulator is flat up to 325 GHz22,25,37. When working at such a high carrier with 3 frequency bands38 one could envision a capacity beyond 180 Gbit/s (see methods section). To sum up, the discussion shows that the suggested scheme has ample margin and a bandwidth-distance

product of as much as e.g. 9 THz·m is surely doable. This could for instance be achieved by the aforementioned 180 Gbit/s QPSK link if transmitted over a distance of 100 m.

Other opportunities will emerge with the rise of phased-array beam steering technologies39. The microwave plasmonic scheme offers a unique advantage as it scales well both in footprint and speed. The scaling is due to the fact that the receiving antenna is extremely compact and may operate up to highest carrier frequencies.

In conclusion, to the best of our knowledge, we have demonstrated the first transparent fibre-wireless link with an entirely integrated direct wireless-to-optical receiver. Key to this was a novel plasmonic mixer which can directly convert a wireless 60 GHz signal to the optical domain. Line rates of 20 Gbit/s were successfully transmitted across a 1 m free-space RF link and up to 5 m at 10 Gbit/s. The receiver is as compact as 0.315 mm^2 which makes it potentially attractive for use in next generation wireless and phased-array systems.

Method

Plasmonic phase modulator

The plasmonic phase modulator (PPM) is based on a metal-insulator-metal slot (see supplementary information, Fig. S1a) guiding surface plasmon polaritons (SPP)28. SPPs are electromagnetic waves propagating along a metal-dielectric interface coupled to charge oscillations at the metal surface. Due to their electronic nature, the spatial wavelength of SPPs is reduced and can therefore be confined to dimensions much smaller than their angular wavelength. By placing two metal-insulator interfaces close to each other, two SPPs can couple to each other to form so-called gap or slot SPPs28. Such metal-insulator-metal (MIM) slot waveguides can strongly confine and guide infrared SPPs. The insulator forming our MIM slot consist of a nonlinear optical (NLO) material. The NLO material used here is composed of organic electro-optic chromophores with a strong $\chi^{(2)}$ nonlinear response. If an electric field is applied across the NLO material, a change is induced in the material's refractive index. This way the phase of propagating SPPs along the MIM slot can be controlled with an external electrical signal. The induced phase shift $\Delta\varphi = \Delta n_{\mathrm{eff}} \cdot L \cdot 2\pi/\lambda$ is proportional to the change in effective refractive index Δn_{eff} and device length L. The effective refractive index change can be expressed as27,40

$$\Delta n_{\mathrm{eff}} = \Gamma \frac{\Delta n_{\mathrm{mat}}}{n_{\mathrm{mat}}} n_{\mathrm{slow}} = \frac{1}{2} n_{\mathrm{mat}}^2 r_{33} \Gamma n_{\mathrm{slow}} E_{\mathrm{slot}}$$

where n_{mat} is the material refractive index, Γ is the confinement factor, n_{slot} the slow down factor, r_{33} the nonlinear coefficient of the electro-optic material and E_{slot} the electric field in the slot. Several factors make the modulation of the SPP's phase efficient40. The perfect confinement in the plasmonic slot of the optical and electrical fields (see supplementary information, Fig. S1b) results in their almost perfect overlap, yielding a high Γ. The bound nature of SPP fields to metals leads to a slow down effect n_{slot} increasing the nonlinear interaction for the same optical path. In addition, the plasmonic slot allows to choose arbitrary nonlinear materials. Organic electro-optic chromophores have been shown to have

very strong electro-optic nonlinearities r_{33}. The nano-scale dimension of the plasmonic slot results in high fields for low applied voltages. These lead to optimal nonlinear interactions and most efficient conversion efficiencies such that Δn_{eff} close to 0.1 can be found40. In addition, the subwavelength nature of the plasmonic slot enables the most compact solution reducing the resistance-capacitance (RC) product of the device. This allows for largest electro-optic bandwidths.

Fibre-to-device coupling

Grating couplers (GC) and silicon (Si) access waveguides are used to couple the optical signal from the optical fibre to the plasmonic modulator and back to the fibre. The GCs couple the optical mode from the fibre to the Si waveguides. The GCs are formed by a periodic arrangement of Si tranches matching the wavelength to couple, e.g. 1550 nm. Subsequently, the optical energy is coupled from the Si waveguide to the plasmonic section via photonic-plasmonic converters (PPC)26,41. The PPC consists of a tapered Si waveguide and inverted metal taper. The evanescent optical field from the Si waveguide couples on both sides to SPPs at the metal interface. At the beginning of the plasmonic slot, both SPPs couple together to form a slot SPP.

Device fabrication

Devices were fabricated on a silicon-on-insulator (SOI) wafer with 220 nm thick silicon layer and 3 μm thick buried oxide. Silicon waveguides with a width of 450 nm and height of 220 nm were patterned by e-beam lithography and dry etching. The waveguides were covered with a 500 nm SiO_2 cladding. Next, the metal forming the plasmonic modulator and antenna arms were deposited by e-beam evaporation and a lift-off process. Finally, a nonlinear optical organic material composite (HD-BB-OH/YLD124) was applied by spin-coating29. The mesoscopic nonlinearity of the organic material was then activated by a poling procedure31. The total device is 900 μm in length and 350 μm wide. The plasmonic slot is 75 nm wide and 17.5 μm in length. For one set of devices, the silicon substrate was thinned down to 250 μm and gold was sputtered on the back of the chip as a back reflector (BR). Note that the device with thinned down substrate was used for the 1 m link experiment. The additional processing on the substrate introduced some additional losses. For this reason, the 5 m link experiment was done with a device without processing of the substrate (no BR).

Electro-optic characterization

Laser light at 1550 nm was coupled to the chip by means of GC. A 60 GHz RF signal generated by a microwave synthesizer is transmitted with a horn antenna onto the chip and used to induce a modulation onto the optical carrier. The optical signal is then analysed with an optical spectrum analyser (OSA) and the electro-optic response of the side bands are measured.

Fibre-wireless-fibre link demonstration

A transparent fibre-wireless-fibre link has been built, see Fig. 3. First, a QPSK signal with a random bit sequence is encoded onto a 1550 nm optical carrier (f_0) with an IQ modulator.

Europe PMC Funders Author Manuscripts

The data signal has a symbol rate between 1 GBd and 10 GBd and is pulse shaped with a square root raised cosine with a roll-off factor of 0.05. In the RF front-end the data signal is combined with a second laser (f_0-f_{ref}) which is tuned for a wavelength offset corresponding to the RF carrier frequency, i.e. 60 GHz. This RF carrier is chosen due to the available equipment. Subsequently, the RF signal is generated using a high-speed (70 GHz) photodetector (Finisar XPDV3120R) with a DC responsivity of 0.6 A/W. With a delivered input optical power of 10 mW, a generated RF power of 1 mW is estimated. For comparison, typical FTTH networks use down-stream optical power levels on the order of 3 mW to support 1.2 Gbit/s. With powers in the same order of magnitude (10 mW) we achieve data rates approximately ten fold higher. To maximize the opto-electrical conversion efficiency, both laser amplitudes are kept at equal powers, see Fig. 3 inset (I). The generated RF signal is then amplified by a high power V-band amplifier (SAGE SBP-5536533022-1515-E1) providing an unsaturated gain of 30 dB, a saturation output power of 22 dBm and an electrical bandwidth of 55-65 GHz. The amplified RF signal is fed to a phased array antenna (Huber&Suhner SENCITY®Matrix) with a gain of 38 dBi and a bandwidth of 57-66 GHz. To overcome the free-space path losses, a HDPE lens is used to focus the MMW energy onto the chip. The lens gain at 60 GHz was measured to be 18 dB. The wireless link between the transmitter and receiver was set first to 1 m. In a second step, the link was increased to 5 m. As an optical table was needed for the receiver setup, the wireless distance was limited by the distance between the optical tables in the laboratory.

The wireless signal containing the data information was then directed to the passive plasmonic mixer. An optical cw signal (f_0-f_{ref}) was coupled into the plasmonic mixer as a new optical carrier on the receiver side. The impinging RF field modulated the laser, and light with the encoded information was coupled out of the receiver chip through the GCs. Subsequently, the optical signal was optically amplified in an EDFA and fed to an optical coherent receiver. The local oscillator (LO) of the coherent receiver was set to the wavelength of one of the sidebands, i.e. corresponding to the wavelength in the optical transmitter (f_0). Offline digital signal processing was then performed at the receiver including matched filtering, timing and carrier recovery, and linear and nonlinear equalization.

Potential of the concept to extend reach and bandwidth

Several issues can be addressed to increase the transmission link and bandwidth. So for instance, one can improve the antenna gain in the transmitter or improve the lens gain in the receiver. The current antenna link gain of transmitter and receiver amounts to a 56 dBi. Yet, 30 dB higher transmitter-receiver gains and beyond have been reported at higher frequencies4,8,34. Another issue to be addressed are the total losses of the chips. For the two generations of chip with and without a reflector we measured total chip losses of 44 and 34 dB. These losses can be attributed to fiber-to-chip coupling losses in the order of 20 and 18 dB, silicon waveguide propagation losses in the order of 10 and 2 dB and losses in the active plasmonic section in the order of 14 and 12 dB, for the two chip generations respectively. Admittedly, these losses are high and could be as low as 8 dB if fabrication would be performed with state-of-the art silicon photonics fabs. In fact, state-of-the–art optical grating couplers offered by industrial fabs guarantee coupling losses in the order of 2.5 dB per

Europe PMC Funders Author Manuscripts

coupler35 while losses for silicon waveguides are well below 1 dB/cm. Also the losses in the active plasmonic section can be reduced. Recently, we were able to introduce a more efficient resonant plasmonic modulation scheme, where losses have been reduced to 2.5 dB36. Thus, by replacing the coupling schemes and implementing the most recent plasmonic modulation schemes the net-optical losses could thus be reduced by up to 26 dB, resulting in an additional 52 dB electrical power in the system. Bringing down these excess losses will allow one to leave out e.g. the electrical amplifier with a 22 dB gain in the transmitter. The additional power could also be used to map higher modulation formats such as 16 QAM onto the optical carrier16 or for transmitting the information across longer distances. Increasing the distance from 5 m to 100 m would for instance require 25 dB out of the loss budget.

Another advantage of the scheme is the scalability to higher carrier frequencies. As the frequency response of plasmonic modulator is flat beyond 300 GHz22,25,37, one could easily resort to a carrier frequency around 300 GHz while preserving the current design with the 10% fractional bandwidth. This would result in an available bandwidth of 30 GHz. In a next step one could arrange e.g. three transmitters in parallel. Parallelization is possible due to the very compact footprint of the device. Assuming 3 frequency bands around 300 GHz with each 30 GHz (typically this will allow the transmission of 30 GBd in each band), one could potentially transmit 3 × 60 Gbit/s of QPSK signals resulting in data rates of up to 180 Gbit/s.

In summary, the current design leaves ample margin for improvement. So there are at least 30 dB of transmitter and receiver link gain and 52 dB of link gain due to optical losses. Further, by transmitting 3 bands of 30 GHz at a carrier of 300 GHz the proposed concept potentially should be able to transmit 180 Gbit/s of data across a wireless distance beyond 100 m. If such a scenario were implemented, it would correspond to a bandwidth distance product of 9 THz·m.

Supplementary Material

Refer to Web version on PubMed Central for supplementary material.

Acknowledgements

This work was carried out partially at the Binnig and Rohrer Nanotechnology Center (BRNC) and in the FIRST lab cleanroom facility at ETH Zurich. We are grateful to H. R. Benedickter and U. Drechsler for the help in the measurement and fabrication, respectively. The EU project ERC PLASILOR (670478) and PLASMOfab (688166) are acknowledged for partial funding of the work. The US National Science Foundation (DMR-1303080) and the Air Force Office of Scientific Research (FA9550-15-1-0319). The ETH Postdoctoral Fellowship (16-2-FEL-51). M. Burla acknowledges the SNSF Ambizione grant (173996).

References

1. Waterhouse R, Novak D. Realizing 5G: Microwave Photonics for 5G Mobile Wireless Systems. IEEE Microw Mag. 2015; 16:84–92.
2. Capmany J, Novak D. Microwave photonics combines two worlds. Nature Photon. 2007; 1:319–330.
3. Yao J. Microwave photonics. J Lightw Technol. 2009; 27:314–335.

4. Nagatsuma T, Ducournau G, Renaud CC. Advances in terahertz communications accelerated by photonics. Nature Photon. 2016; 10:371–379.
5. Seeds AJ, Shams H, Fice MJ, Renaud CC. TeraHertz Photonics for Wireless Communications. J Lightw Technol. 2015; 33:579–587.
6. Lim C, et al. Fiber-Wireless Networks and Subsystem Technologies. J Lightw Technol. 2010; 28:390–405.
7. Shams H, Seeds A. Photonics, Fiber and THz Wireless Communication. Opt Photon News. 2017; 28:24–31.
8. Koenig S, et al. Wireless sub-THz communication system with high data rate. Nature Photon. 2013; 7:977–981.
9. Ducournau G, et al. Ultrawide-bandwidth single-channel 0.4-THz wireless link combining broadband quasi-optic photomixer and coherent detection. IEEE Trans Terahertz Sci Technol. 2014; 4:328–337.
10. Yu X, et al. 400-GHz Wireless Transmission of 60-Gb/s Nyquist-QPSK Signals Using UTC-PD and Heterodyne Mixer. IEEE Trans Terahertz Sci Technol. 2016; 6:765–770.
11. Ito H, Nakajima F, Furuta T, Ishibashi T. Continuous THz-wave generation using antenna-integrated uni-travelling-carrier photodiodes. Semicond Sci Technol. 2005; 20:S191.
12. Yardimci NT, Cakmakyapan S, Hemmati S, Jarrahi M. A High-Power Broadband Terahertz Source Enabled by Three-Dimensional Light Confinement in a Plasmonic Nanocavity. Sci Rep. 2017; 7 4166.
13. Renaud CC, et al. Antenna Integrated THz Uni-Traveling Carrier Photodiodes. IEEE J Sel Top Quantum Electron. 2018; 24:1–11.
14. Li X, Yu J, Xiao J, Xu Y. Fiber-Wireless-Fiber Link for 128-Gb/s PDM-16QAM Signal Transmission at *W*-Band. IEEE Photon Technol Lett. 2014; 26:1948–1951.
15. Marpaung D, et al. Integrated microwave photonics. Laser Photonics Rev. 2013; 7:506–538.
16. Yang C, Li X, Xiao J, Chi N, Yu J. Fiber-wireless integration for 80 Gbps polarization division multiplexing– 16QAM signal transmission at W-band without RF down conversion. Microw Opt Technol Lett. 2015; 57:9–13.
17. Wijayanto YN, Murata H, Okamura Y. Electrooptic Millimeter-Wave-Lightwave Signal Converters Suspended to Gap-Embedded Patch Antennas on Low-*k* Dielectric Materials. IEEE J Sel Top Quantum Electron. 2013; 19:33–41.
18. Zhang X, et al. Integrated Photonic Electromagnetic Field Sensor Based on Broadband Bowtie Antenna Coupled Silicon Organic Hybrid Modulator. J Lightw Technol. 2014; 32:3774–3784.
19. Park D, et al. RF photonic downconversion of vector modulated signals based on a millimeter-wave coupled electrooptic nonlinear polymer phase-modulator. Opt Express. 2017; 25:29885–29895. [PubMed: 29221024]
20. Chung CJ, et al. Silicon-Based Hybrid Integrated Photonic Chip for K u band Electromagnetic Wave Sensing. J Lightw Technol. 2018; 36:1568–1575.
21. Brongersma ML, Shalaev VM. The Case for Plasmonics. Science. 2010; 328:440–441. [PubMed: 20413483]
22. Hoessbacher C, et al. Plasmonic modulator with >170 GHz bandwidth demonstrated at 100 GBd NRZ. Opt Express. 2017; 25:1762–1768. [PubMed: 29519029]
23. Baeuerle B, , et al. Optical Fiber Communication Conference; Optical Society of America; 2018. M2I.1
24. Gramotnev DK, Bozhevolnyi SI. Plasmonics beyond the diffraction limit. Nature Photon. 2010; 4:83.
25. Benea-Chelmus I-C, et al. Three-Dimensional Phase Modulator at Telecom Wavelength Acting as a Terahertz Detector with an Electro-Optic Bandwidth of 1.25 Terahertz. ACS Photon. 2018; 5:1398–1403.
26. Haffner C, et al. Plasmonic organic hybrid modulators—scaling highest speed photonics to the microscale. Proc IEEE. 2016; 104:2362–2379.
27. Salamin Y, et al. Direct Conversion of Free Space Millimeter Waves to Optical Domain by Plasmonic Modulator Antenna. Nano Lett. 2015; 15:8342–8346. [PubMed: 26570995]

28. Pile DFP, et al. Two-dimensionally localized modes of a nanoscale gap plasmon waveguide. Applied Physics Letters. 2005; 87 261114.
29. Elder DL, et al. Effect of Rigid Bridge-Protection Units, Quadrupolar Interactions, and Blending in Organic Electro-Optic Chromophores. Chem Mater. 2017; 29:6457–6471.
30. Woo I, Nguyen TK, Han H, Lim H, Park I. Four-leaf-clover-shaped antenna for a THz photomixer. Opt Express. 2010; 18:18532–18542. [PubMed: 20940745]
31. Heni W, et al. Nonlinearities of organic electro-optic materials in nanoscale slots and implications for the optimum modulator design. Opt Express. 2017; 25:2627–2653. [PubMed: 29519106]
32. Mokhtari-Koushyar F, et al. Wideband Multi-Arm Bowtie Antenna for Millimeter Wave Electro-Optic Sensors and Receivers. J Lightw Technol. 2018; 36:3418–3426.
33. Chang F, Onohara K, Mizuochi T. Forward error correction for 100 G transport networks. IEEE Communications Magazine. 2010; 48:S48–S55.
34. Kallfass I, et al. 64 Gbit/s Transmission over 850 m Fixed Wireless Link at 240 GHz Carrier Frequency. J Infrared Millim Terahertz Waves. 2015; 36:221–233.
35. Vermeulen D, et al. High-efficiency fiber-to-chip grating couplers realized using an advanced CMOS-compatible Silicon-On-Insulator platform. Opt Express. 2010; 18:18278–18283. [PubMed: 20721220]
36. Haffner C, et al. Low-loss plasmon-assisted electro-optic modulator. Nature. 2018; 556:483–486. [PubMed: 29695845]
37. Ummethala S, , et al. Conference on Lasers and Electro-Optics; Optical Society of America; 2018. STu3D.4
38. Jia S, et al. 120 Gb/s Multi-Channel THz Wireless Transmission and THz Receiver Performance Analysis. IEEE Photon Technol Lett. 2017; 29:310–313.
39. Sun J, Timurdogan E, Yaacobi A, Hosseini ES, Watts MR. Large-scale nanophotonic phased array. Nature. 2013; 493:195–199. [PubMed: 23302859]
40. Haffner C, et al. All-plasmonic Mach–Zehnder modulator enabling optical high-speed communication at the microscale. Nature Photon. 2015; 9:525–528.
41. Tian J, Yu S, Yan W, Qiu M. Broadband high-efficiency surface-plasmon-polariton coupler with silicon-metal interface. App Phys Lett. 2009; 95:13504.

Fig. 1. Prospective application scenario for point to point high-capacity fibre-wireless link.
Deploying the fibre-to-the-home (FTTH) can be costly. One possible scenario reducing the cost, while still providing high-capacity connectivity for the end user is to use virtual fibres (red beams) for the last few meters. Here, optical fibres (yellow lines) are deployed to the residential area either underground or above ground using existing cable platforms. Lamp posts located close to the houses could host optical-to-wireless converters for down-stream (red dashed arrow), and wireless-to-optical converters (plasmonic mixer) for the up-stream data (red dashed arrow). A direct converter could very simply and cost efficiently map the wireless signal onto a common laser signal, which then can be routed back to the central office.

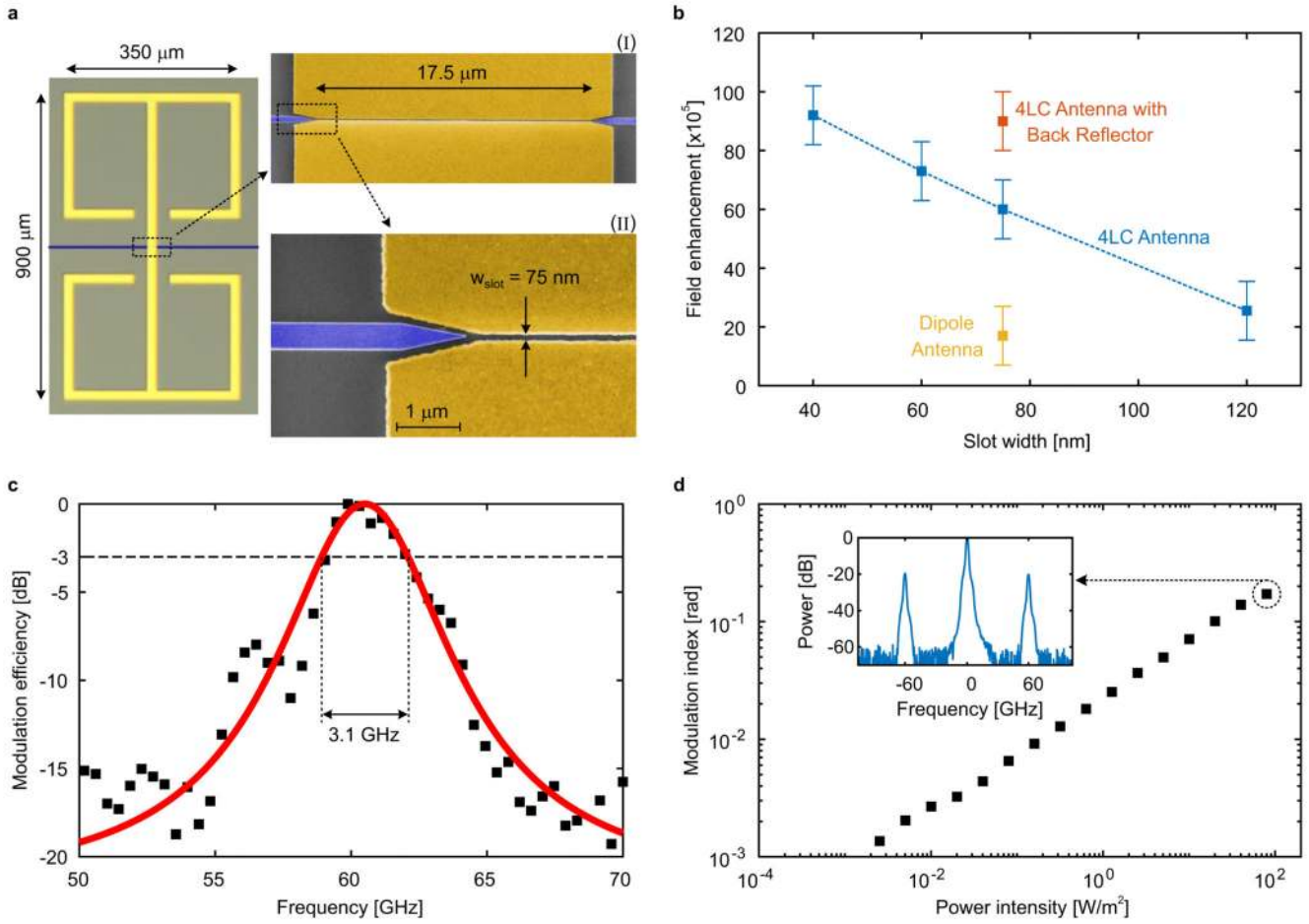

Fig. 2. Device structure and performance.

a, Top view showing an optical microscope image of the four-leaf-clover antenna with the integrated plasmonic phase modulator. Blow-up scanning-electron microscope (SEM) colorized images of the phase-modulator section (I) and detail view of the photonic-to-plasmonic converter (II). **b**, Field enhancement provided by the structure as a function of the slot width. **c**, Electro-optic bandwidth of the plasmonic mixer. **d**, Modulation index as a function of the power intensity at the plasmonic mixer. The measurement is based on a 5 m link. The inset shows the normalized electro-optical response of the plasmonic mixer.

Europe PMC Funders Author Manuscripts

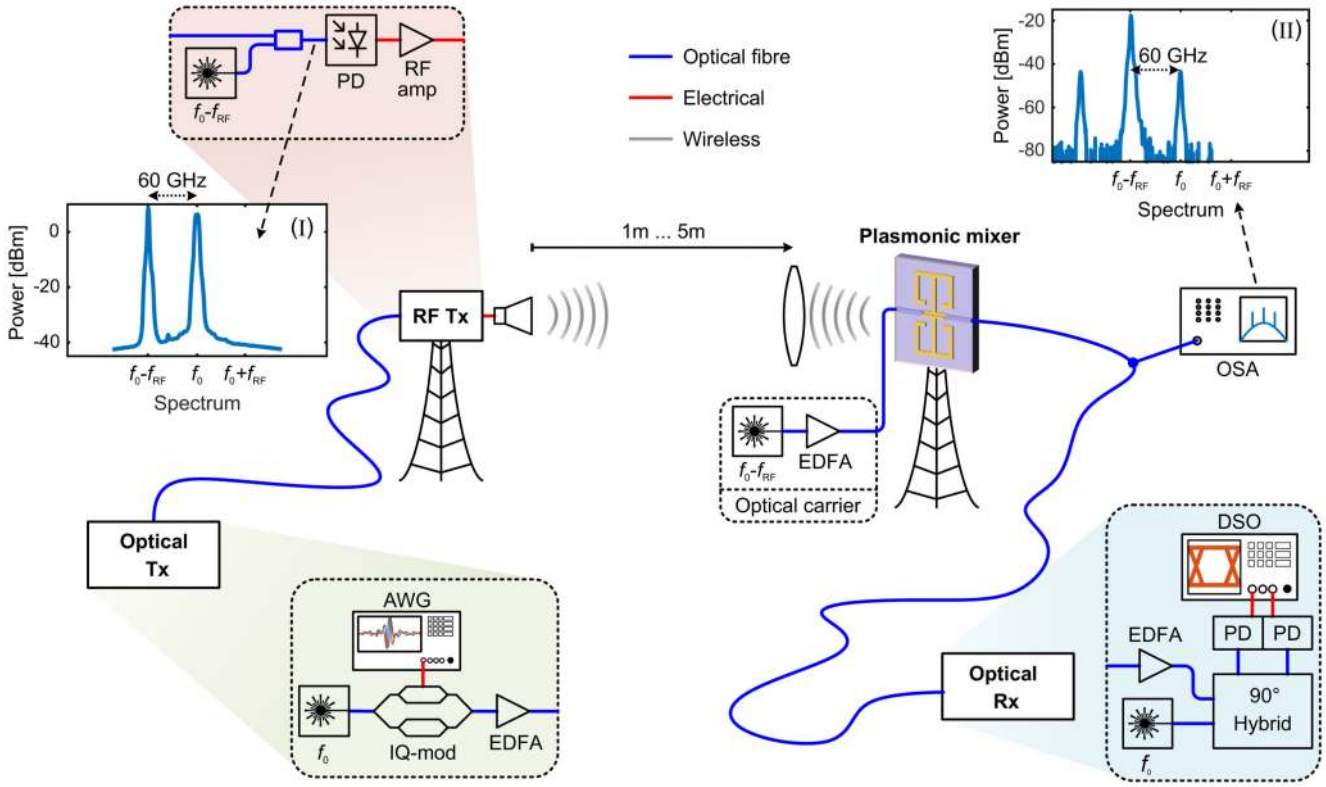

Fig. 3. Fibre-to-wireless and wireless-to-fibre link experiment.

First the optical signal is generated by encoding a QPSK signal with a random bit sequence of length 40960 onto a 1550 nm optical carrier (f_0). The optical signal (10 dBm) is subsequently combined with a reference laser (f_0-f_{RF}) detuned by 60 GHz and fed into a high-speed photodetector. The resulting MMW signal is amplified and emitted to the far-field by a high-gain millimetre-wave antenna. The wireless signal is focused by means of a high-density polyethylene lens onto the plasmonic mixer and converted back to the optical domain. The optical signal is decoded in a coherent receiver system consisting of a 90° hybrid mixer and photodetectors. Tx: transmitter, EDFA: erbium-doped fibre amplifier, PD: photodiode, DSO: real-time digital storage oscilloscope, OSA optical spectrum analyser, RF Amp: radio-frequency power amplifier, IQ-Mod: in-phase and quadrature modulator.

Europe PMC Funders Author Manuscripts

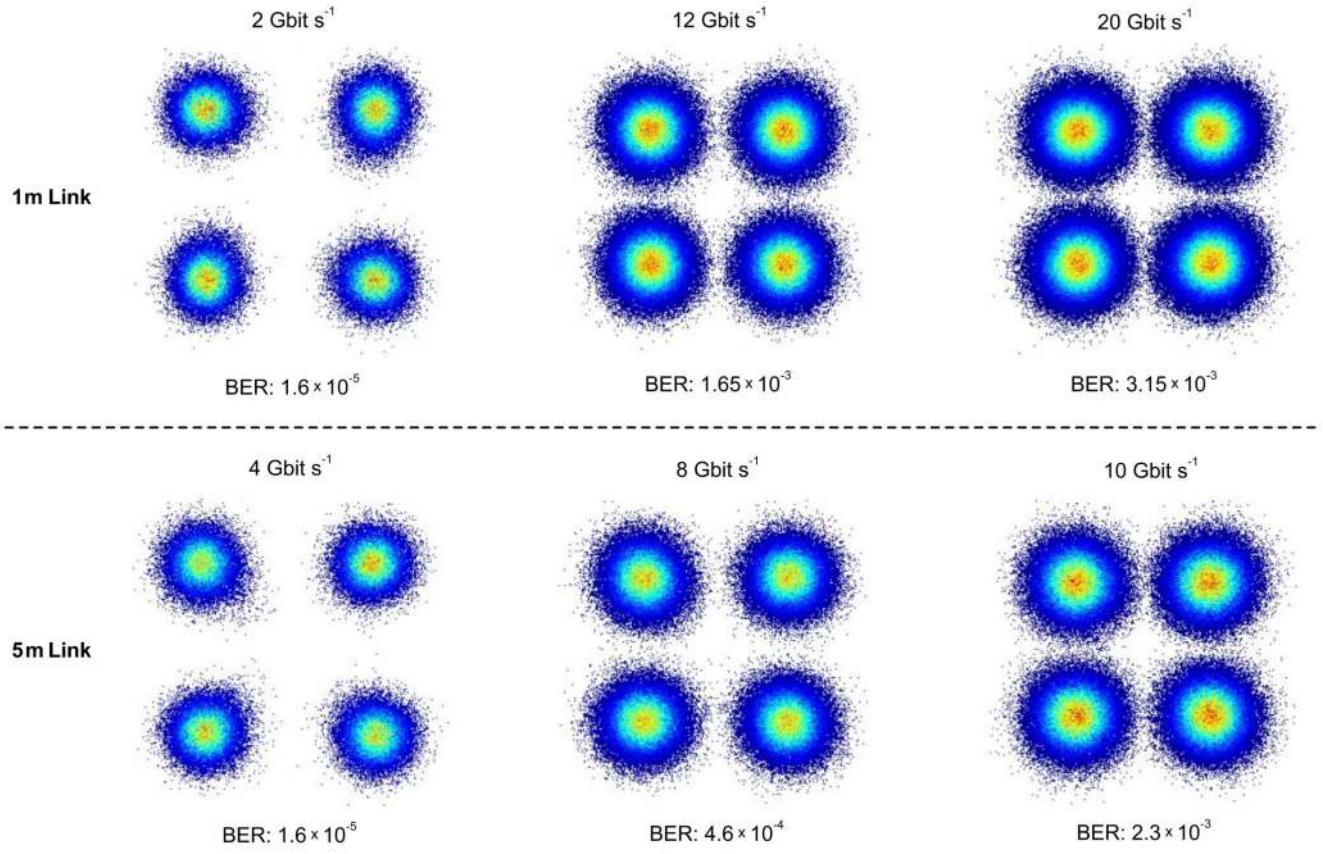

Fig. 4. Experimental results.

Fibre-wireless transmission experiment results for 1 m and 5 m wireless link. Constellation diagrams at 2 Gbit/s, 12 Gbit/s and 20 Gbit/s are shown for a wireless distance of 1 m. For the 5 m wireless link experiment the constellation diagram at 2 Gbit/s, 8 Gbit/s and 10 Gbit/s are shown.

Europe PMC Funders Author Manuscripts